**Supplementary material for**

# Isotopomer labeling and oxygen dependence of hybrid nitrous oxide production

Colette L. Kelly,[1,2*] Nicole M. Travis,[1] Pascale Anabelle Baya,[1] Claudia Frey,[3] Xin Sun,[4] Bess B. Ward,[5] and Karen L. Casciotti[1]

[1]Department of Earth System Science, Stanford University, Stanford, CA 94305, U.S.A.
[2]Department of Marine Chemistry and Geochemistry, Woods Hole Oceanographic Institution, Woods Hole, MA 02543, U.S.A.
[3]Department of Environmental Science, University of Basel, Basel, Switzerland
[4]Department of Global Ecology, Carnegie Institution for Science, Stanford, CA 94305, U.S.A.
[5]Department of Geosciences, Princeton University, Princeton, NJ 08544, U.S.A.

*Correspondence to:* Colette L. Kelly (email: colette.kelly@whoi.edu).

**Contents of this file:**

**Supplemental Figures**

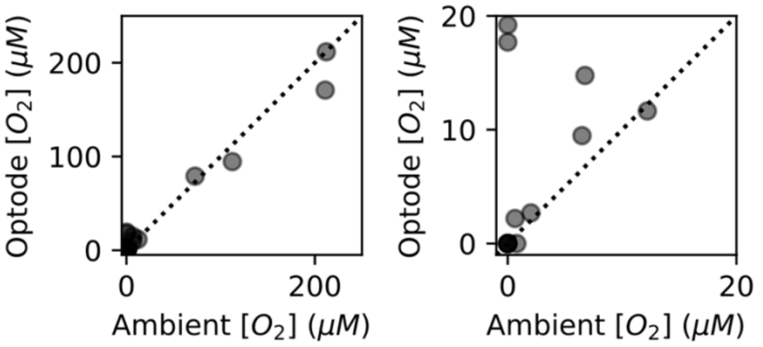


**Figure S1. $[O_2]$ measured by chemiluminescent optodes mounted inside sample bottles vs. ambient $[O_2]$ measured by a Seabird sensor for the bottles from which samples were taken. Data (circles) are plotted along the full range of $[O_2]$ (a) and zoomed in to 0-20 µM $[O_2]$ (b). The dashed line in each plot is the 1:1 line. High values of optode $[O_2]$ at 0 ambient $[O_2]$ correspond to the two experiments at anoxic depths at station PS2 that were not purged before tracer addition.**

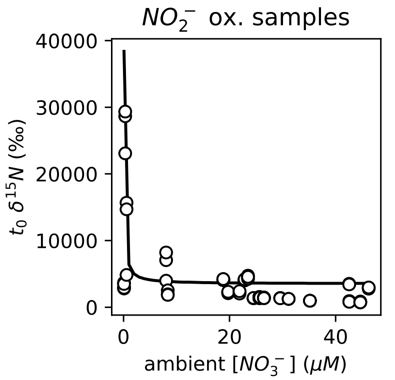


**Figure S2. $\delta$(15N-NOx) at t0 vs. ambient [NO3–] in 15N-NO2– experiments. High t0 $\delta$(15N-NOx) at low ambient [NO3–] suggests that the sulfamic treatment did not remove all of the 15N-NO2– before denitrifier analysis. This should affect each timepoints equally, however, and should not affect the slope of $\delta$(15N-NOx) over the course of the experiment.**

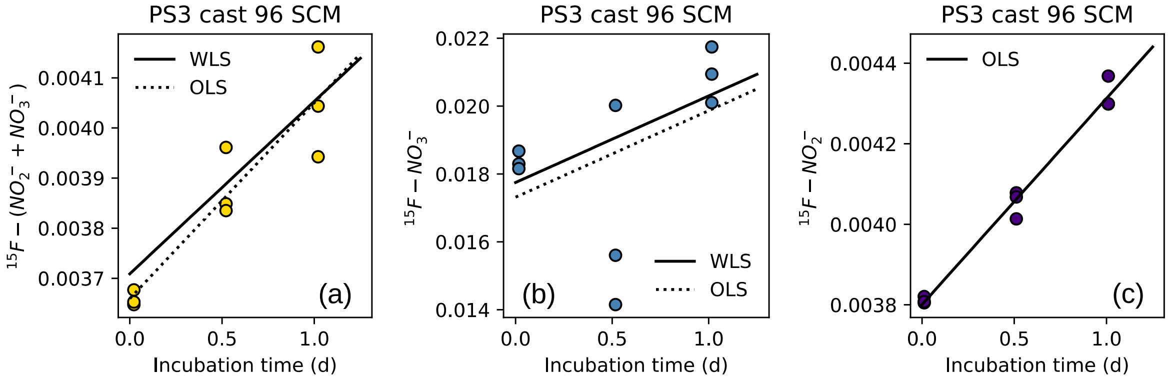


**Figure S3. Example $^{15}$N time course for the $^{15}$N-$NH_4^+$ incubation experiment (a, yellow), $^{15}$N-$NO_2^-$ incubation experiment (b, blue), and $^{15}$N-$NO_3^-$ incubation experiment (c, indigo) in the secondary chlorophyll maximum at station PS3. Rates are calculated from the slope of the production atom fraction vs. incubation time. When production atom fraction was calculated with the denitrifier method ($^{15}$N-$NH_4^+$ and $^{15}$N-$NO_2^-$ experiments), slopes were calculated with a weighted least squares linear regression, weighting each point by its uncertainty. Weighted least squares (dashed line) and ordinary least squares (solid line) slopes are shown in each plot.**

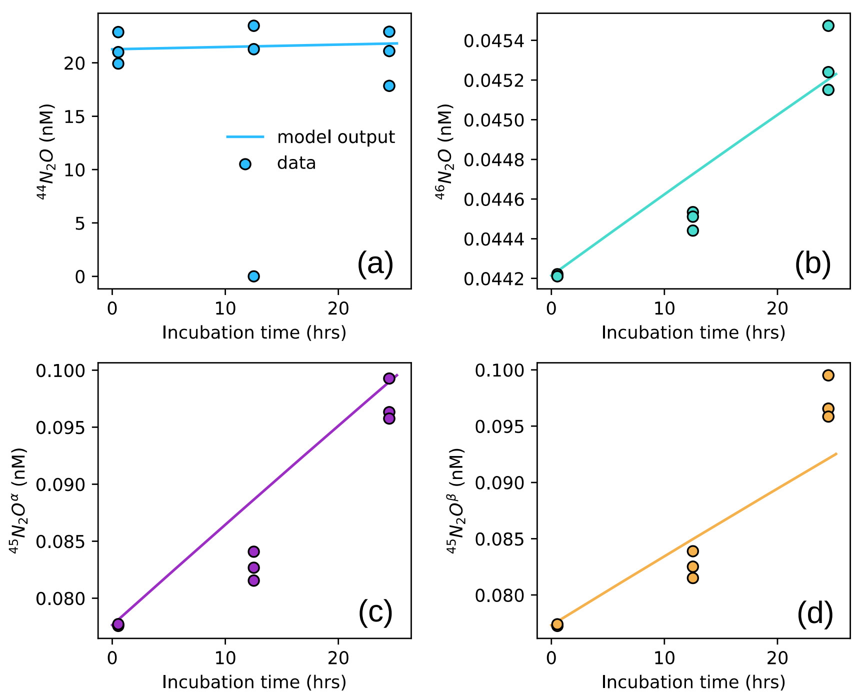


**Figure S4. Example forward-running model fit through $N_2O$ isotopocule data for the $^{15}$N-$NH_4^+$ experiment in the secondary chlorophyll maximum at station PS3. Model output (solid lines) is optimized against the observed $^{46}N_2O$ (a), $^{45}N_2O^{\alpha}$ (b), $^{45}N_2O^{\beta}$ (c), and $^{44}N_2O$ (d) at each timepoint in each tracer experiment.**

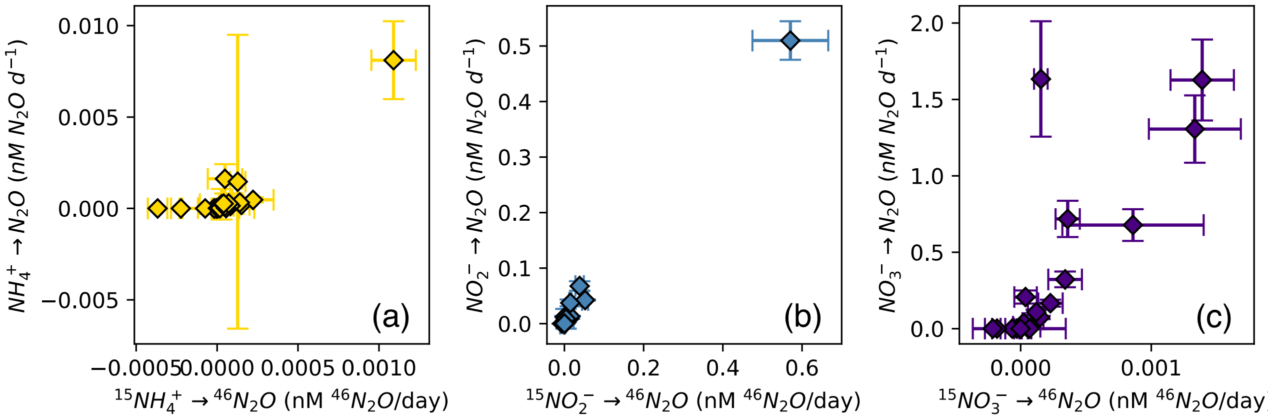


**Figure S5. Modeled $N_2O$ production processes are plotted against net $^{46}N_2O$ production to ground-truth the forward-running model. Total $N_2O$ production from solely $NH_4^+$ is plotted against net $^{46}N_2O$ production from $^{15}N$-$NH_4^+$ (a, yellow); modeled $N_2O$ production from $NO_2^-$ via denitrification is plotted against net $^{46}N_2O$ production from $^{15}N$-$NO_2^-$ (b, blue); and modeled $N_2O$ production from $NO_3^-$ via denitrification is plotted against net $^{46}N_2O$ production from $^{15}N$-$NO_3^-$ (c, indigo) at all stations and depths. The y-axes achieve greater rates than the x-axes because the y-axes represent the total $N_2O$ production from a given process ($^{44}N_2O$+$^{45}N_2O$+$^{46}N_2O$), while the x-axes represent only the net production of $^{46}N_2O$ from a given $^{15}N$-labeled substrate. Since the model cannot produce negative rates, negative net rates of net $^{46}N_2O$ production correspond to modeled $N_2O$ production rates of zero.**

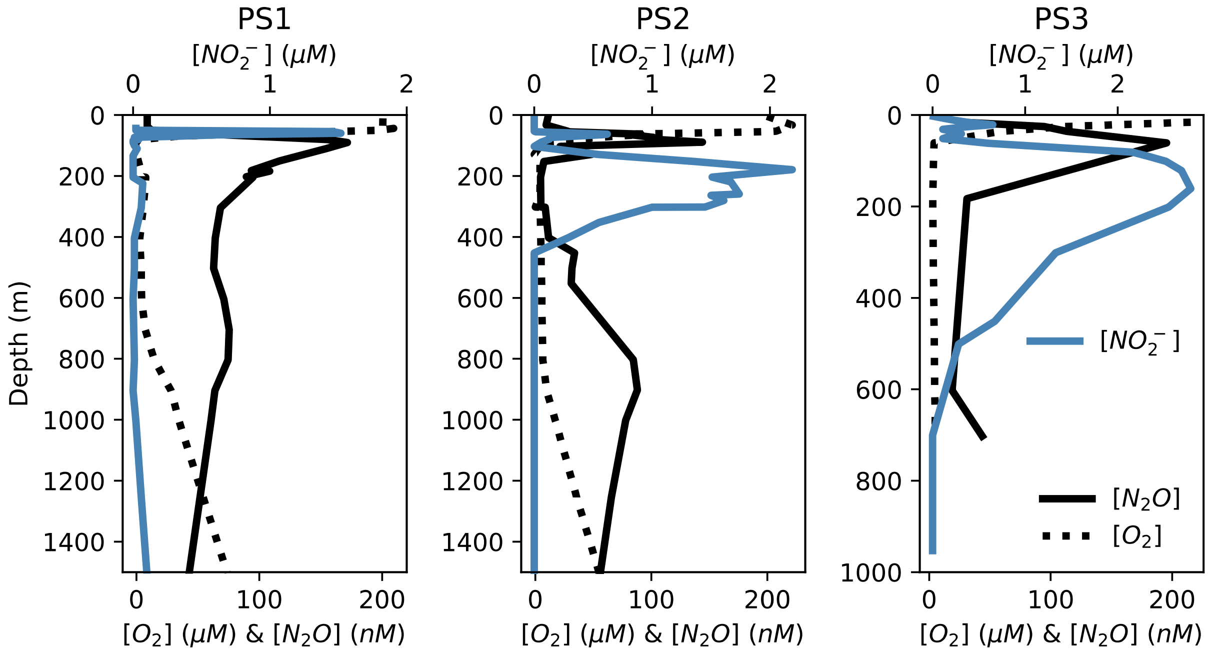


**Figure S6. Dissolved $[O_2]$ (dashed black lines), $[N_2O]$ (solid black lines), and $[NO_2^-]$ (solid blue lines) at station PS1 (a), PS2 (b), and PS3 (c). Data from Kelly et al., 2021.**

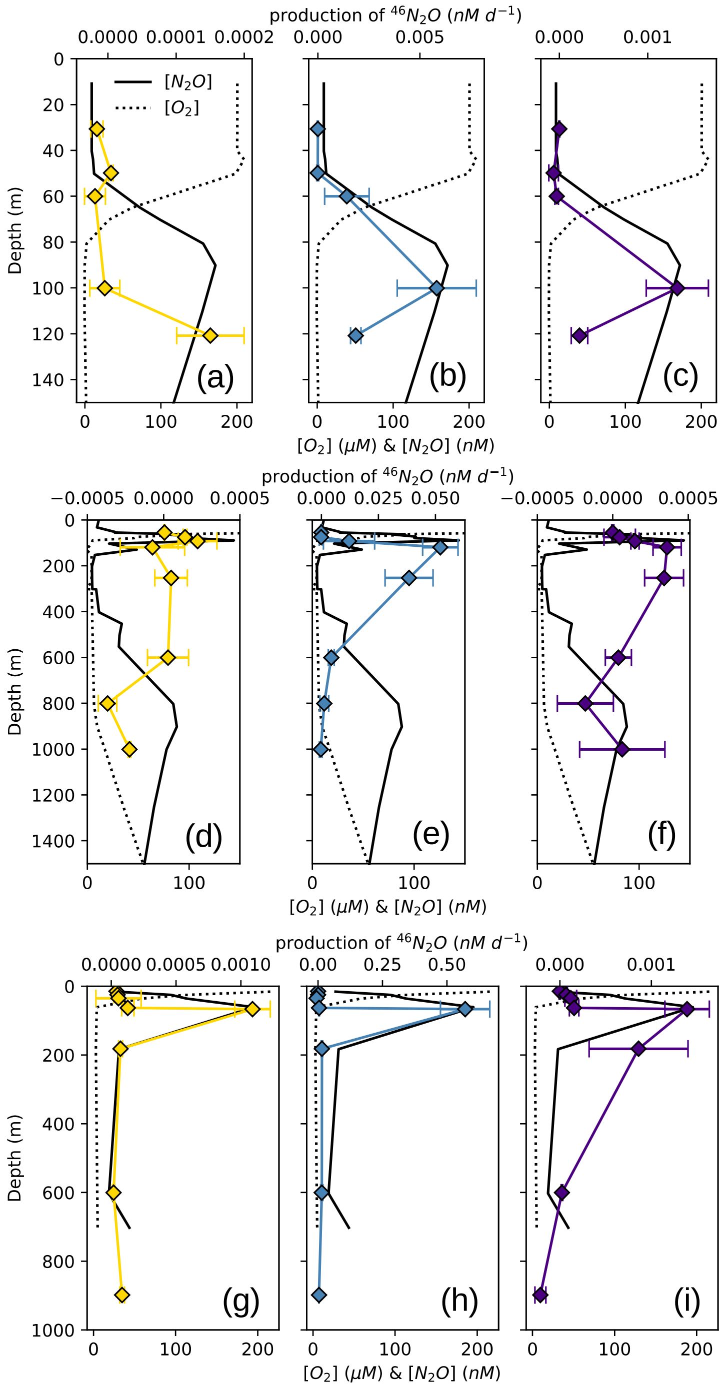


**Figure S7. Net $^{46}N_2O$ production from $^{15}N\text{-}NH_4^+$ (a, d, g, yellow), $^{15}N\text{-}NO_2^-$ (b, e, h, blueo), and $^{15}N\text{-}NO_3^-$ (c, f, i, indigo) at stations PS1 (a-c), PS2 (d-f), and PS3 (g-i). $N_2O$ production rates are plotted over depth profiles of dissolved [$O_2$] (dashed lines) and [$N_2O$] (solid lines, from Kelly et al., 2021). Error bars are calculated from linear regression slope error of $^{46}N_2O$ vs. incubation time. Note the different x-axis scales for $^{46}N_2O$ production (top) and [$O_2$] and [$N_2O$] (bottom).**

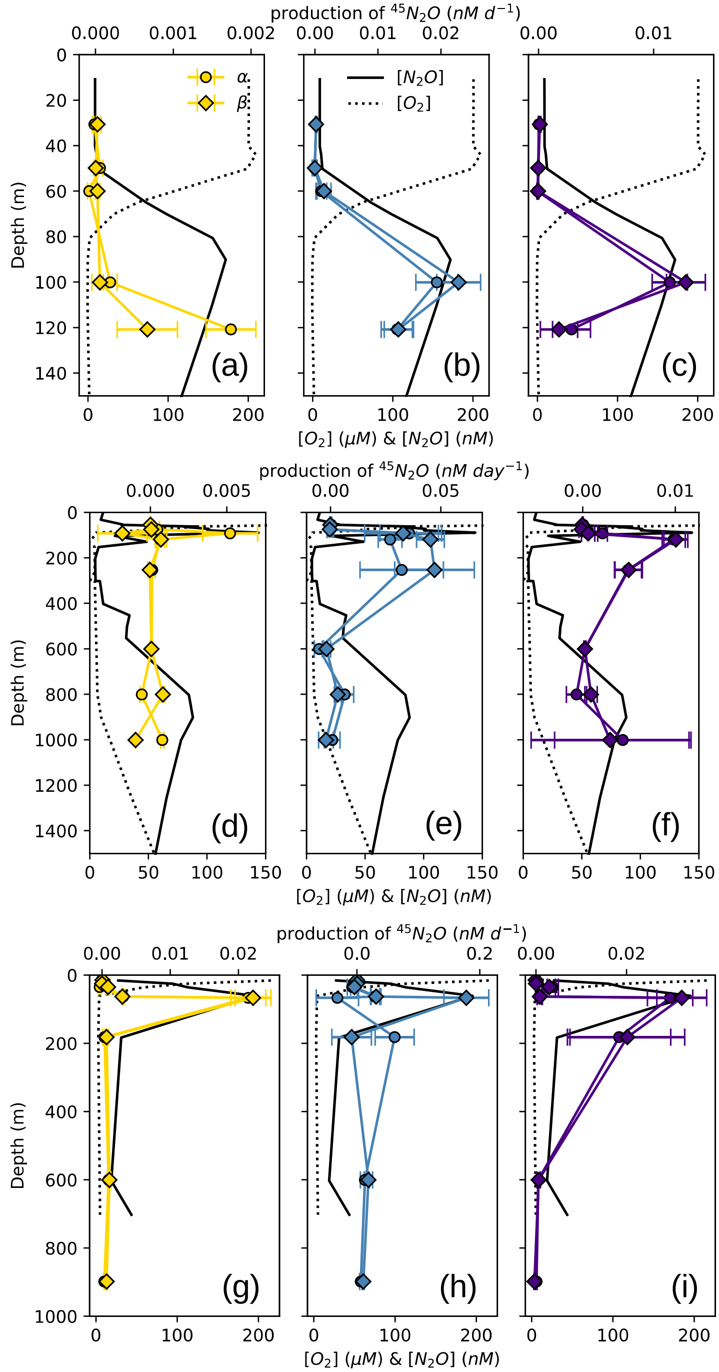


**Figure S8. Net $^{45}N_2O^{\alpha}$ (circles) and $^{45}N_2O^{\beta}$ (diamonds) production from $^{15}N$-$NH_4^+$ (a, d, g, yellow), $^{15}N$-$NO_2^-$ (b, e, h, blue), and $^{15}N$-$NO_3^-$ (c, f, i, indigo) at stations PS1 (a-c), PS2 (d-f), and PS3 (g-i). $N_2O$ production rates are plotted over depth profiles of dissolved $[O_2]$ (dashed lines) and $[N_2O]$ (solid lines, from Kelly et al., 2021). Error bars are calculated from linear regression slope error of $^{45}N_2O$ vs. incubation time. Note the different x-axis scales for $^{45}N_2O$ production (top) and $[O_2]$ and $[N_2O]$ (bottom).**

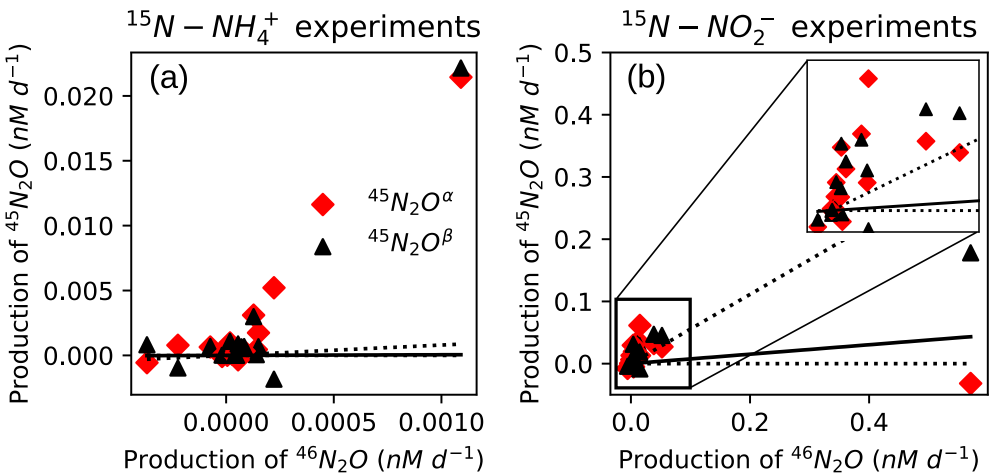


**Figure S9. Net production of $^{45}N_2O^{\alpha}$ (red diamonds) and $^{45}N_2O^{\beta}$ (black triangles) vs. $^{46}N_2O$ from $^{15}N$-$NH_4^+$ (a) and $^{15}N$-$NO_2^-$ (b). The insert in (b) shows a zoomed-in view of the data. The solid black lines indicate the expected production $^{45}N_2O^{\alpha}$ and $^{45}N_2O^{\beta}$ from a process drawing both N atoms in $N_2O$ from the same substrate pool, based on the atom fraction of the labeled substrate ($NH_4^+$ or $NO_2^-$) and a binomial distribution of $N_2O$ isotopocules. Dashed lines indicate the range of expected values, based on the range of atom fractions in each experiment. Production of $^{45}N_2O^{\alpha}$ and $^{45}N_2O^{\beta}$ above this expected production indicate the presence of a hybrid process.**

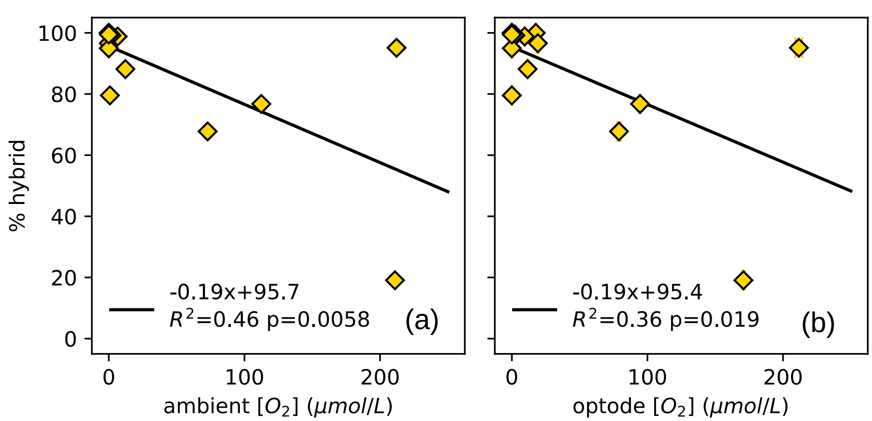


**Figure S10. Hybrid production as a percentage of $N_2O$ production from $NH_4^+$ along a range of ambient [O2] measured by a Seabird sensor for the Niskin bottles from which samples were taken (a) and [$O_2$] measured by chemiluminescent optodes mounted inside sample bottles (b). Slope, intercept, $R^2$, and p-values are displayed on each plot for the ordinary least squares regression through the data.**

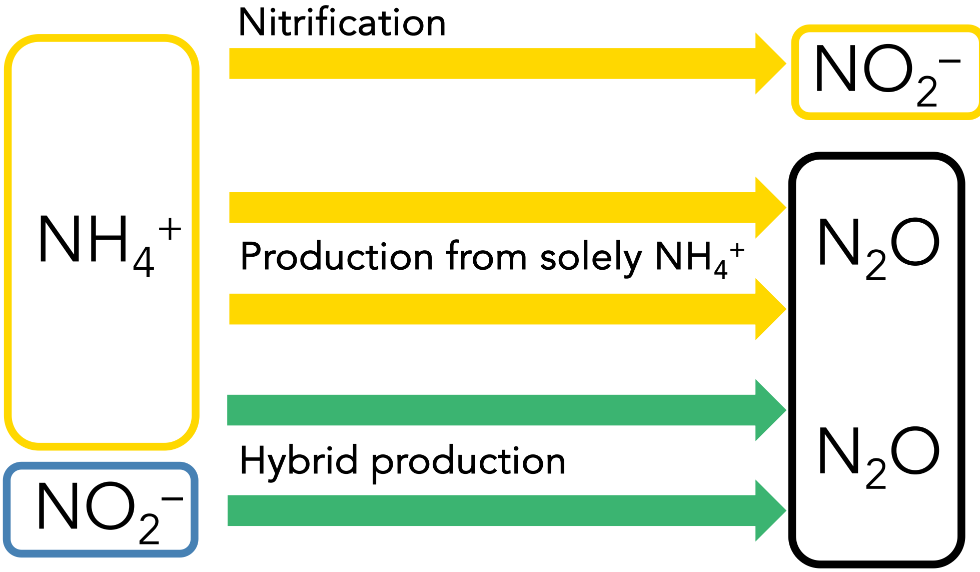


**Figure S11. To ensure mass balance in terms of $NH_4^+$ consumption, $N_2O$ yield (%) during production from $NH_4^+$ is calculated as {2*($N_2O$ production from $NH_4^+$, nM $N_2O$ /day) /[2*($N_2O$ production from $NH_4^+$, nM $N_2O$ /day) + hybrid $N_2O$ production, nM $N_2O$ /day + $NH_4^+$ oxidation, nM N/day]}*100. $N_2O$ yield (%) during hybrid production is calculated as {hybrid $N_2O$ production, nM $N_2O$ /day /[2*($N_2O$ production from $NH_4^+$, nM $N_2O$ /day) + hybrid $N_2O$ production, nM $N_2O$ /day + $NH_4^+$ oxidation, nM N/day]}*100.**

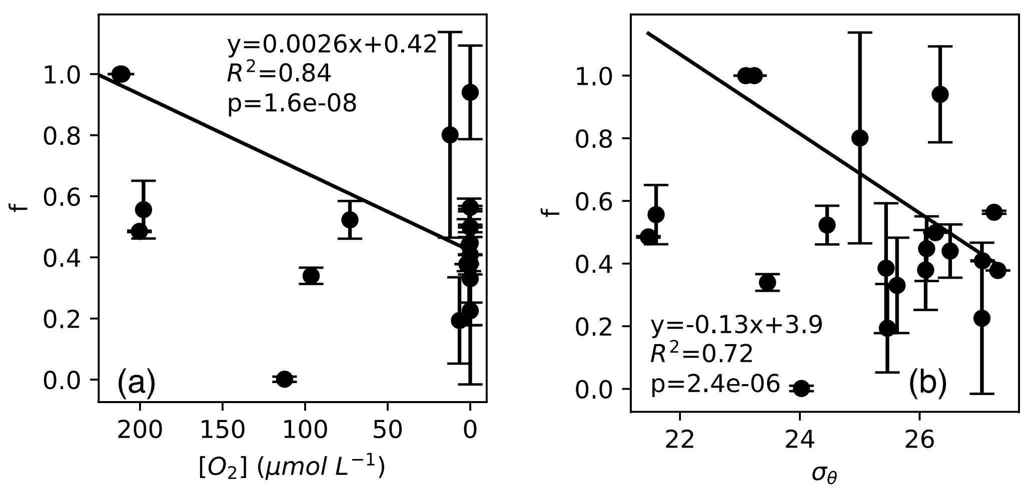


**Figure S12. Weighted least squares regressions of *f* against ambient $[O_2]$ (a) and ambient $[NO_2^-]$ (b). Slope, intercept, $R^2$, and p-values are displayed on each plot for the weighted least squares regression through the data. The value of *f* indicates the proportion of each N atom in $N_2O$ derived from $NH_4^+$ and $NO_2^-$ during hybrid $N_2O$ production; as approaches 1, more of $N^\alpha$ is derived from $NO_2^-$. Separation of $^{45}N_2O^\alpha$ and $^{45}N_2O^\beta$ production indicate values of *f* less than or greater than ½.**

**Table S1. CTD bottle data, ambient nutrient concentrations, and optode [$O_2$] measurements for each experimental depth. Optode [$O_2$] is calculated from the mean $O_2$ measured by chemiluminescent optodes at each of three timepoints.**

| Station | Feature description | Feature abbreviation | Longitude (W) | Latitude [N] | CTD Pressure [db] | CTD Depth [m] | Sigma theta [kg/m3] | CTD Salinity [psu] | CTD Temperature [C] | PAR [µE/m2/s] | Seabird $O_2$ [umol/L] | $NO_3^-$ [uM] | $NO_2^-$ [uM] | $NH_4^+$ [nM] | Optode $O_2$ [umol/L] | Optode $O_2$ stdev [umol/L] |
|---|---|---|---|---|---|---|---|---|---|---|---|---|---|---|---|---|
| PS1 | Upper oxic-anoxic interface | Interface | 113.00 | 10.00 | 100.71 | 100.11 | 26.12 | 34.79 | 13.59 | 0.00 | 0.00 | 29.56 | 0.01 | 3.70 | | |
| | Midpoint of upper oxycline | Mid-oxycline | 113.00 | 10.00 | 60.37 | 60.02 | 23.46 | 34.28 | 22.75 | 0.80 | 96.35 | 8.35 | 1.07 | 8.75 | | |
| | Secondary chlorophyll max. | SCM | 113.00 | 10.00 | 121.55 | 120.82 | 26.26 | 34.80 | 12.90 | 0.49 | 0.00 | 31.13 | 0.02 | 2.14 | | |
| | Mixed layer | Surface | 113.00 | 10.00 | 30.83 | 30.65 | 21.47 | 33.68 | 27.79 | 371.78 | 200.34 | 0.10 | 0.02 | 0.00 | | |
| | Top of upper oxycline | Top of oxycline | 113.00 | 10.00 | 50.15 | 49.86 | 21.60 | 33.68 | 27.39 | 2.31 | 197.86 | 0.09 | 0.74 | 89.79 | | |
| PS2 | Top of deep oxycline below ODZ | Base of ODZ | 105.00 | 15.77 | 807.19 | 800.88 | 27.24 | 34.54 | 5.67 | 0.02 | 0.00 | 42.58 | 0.00 | 2.62 | 17.70 | 0.11 |
| | ODZ core, deep | Deep ODZ core | 105.00 | 15.77 | 605.20 | 600.77 | 27.04 | 34.56 | 7.27 | 0.02 | 0.00 | 35.16 | 0.00 | 4.76 | 19.20 | 0.83 |
| | Within deep oxycline below ODZ | Deep oxycline | 105.00 | 15.77 | 1009.58 | 1001.21 | 27.36 | 34.54 | 4.62 | 0.02 | 6.75 | 44.66 | 0.00 | 1.62 | 14.77 | 0.17 |
| | Upper oxic-anoxic interface | Interface | 105.00 | 15.77 | 92.85 | 92.28 | 25.46 | 34.64 | 16.48 | 7.96 | 6.49 | 25.63 | 0.10 | 12.95 | 9.48 | 0.09 |
| | Primary nitrite max. | PNM | 105.00 | 15.77 | 75.61 | 75.15 | 24.46 | 34.43 | 19.51 | 29.49 | 72.84 | 19.73 | 0.13 | 12.20 | 79.05 | 1.26 |
| | Secondary chlorophyll max. | SCM | 105.00 | 15.77 | 126.03 | 125.25 | 25.98 | 34.76 | 14.14 | 0.21 | 0.00 | 26.24 | 0.30 | 50.00 | 0.00 | 0.03 |
| | Secondary nitrite max. | SNM | 105.00 | 15.77 | 254.90 | 253.25 | 26.51 | 34.74 | 11.38 | 0.03 | 0.80 | 24.52 | 1.74 | 3.86 | 0.00 | 0.04 |
| | Top of upper oxycline | Top of oxycline | 105.00 | 15.77 | 55.11 | 54.78 | 23.24 | 34.58 | 24.30 | 170.50 | 212.14 | 0.58 | 0.01 | 34.80 | 211.69 | 2.57 |
| PS3 | ODZ core, deep | Deep ODZ core | 102.35 | 17.68 | 604.84 | 600.35 | 27.05 | 34.57 | 7.28 | 0.02 | 0.00 | 42.55 | 0.28 | 5.26 | 0.00 | 0.01 |
| | Within deep oxycline below ODZ | Deep oxycline | 102.35 | 17.68 | 905.62 | 898.25 | 27.30 | 34.55 | 5.19 | 0.02 | 2.03 | 46.23 | 0.00 | 9.00 | 2.69 | 0.03 |
| | Oxic-anoxic interface, cast 87 | Interface | 102.35 | 17.68 | 39.94 | 39.70 | 24.96 | 34.61 | 18.08 | 0.03 | 12.48 | 18.81 | 0.23 | 6.35 | 11.65 | 0.04 |
| | Oxic-anoxic interface, cast 100 | Interface2 | 102.35 | 17.68 | 63.26 | 62.87 | 25.44 | 34.71 | 16.39 | 0.03 | 0.64 | 23.47 | 0.60 | 15.85 | 2.20 | 0.03 |
| | Midpoint of upper oxycline | Mid-oxycline | 102.35 | 17.68 | 24.89 | 24.74 | 24.03 | 34.46 | 21.21 | 0.03 | 112.42 | 8.03 | 0.33 | 12.39 | 94.56 | 0.25 |
| | Secondary chlorophyll max. | SCM | 102.35 | 17.68 | 63.32 | 62.93 | 25.64 | 34.76 | 15.64 | 0.03 | 0.00 | 22.83 | 0.60 | 15.85 | 0.00 | 0.01 |
| | Secondary nitrite max. | SNM | 102.35 | 17.68 | 182.91 | 181.74 | 26.34 | 34.82 | 12.57 | 0.03 | 0.00 | 21.88 | 2.67 | 4.18 | 0.00 | 0.01 |
| | Top of upper oxycline | Top of oxycline | 102.35 | 17.68 | 14.68 | 14.60 | 23.10 | 34.51 | 24.59 | 0.07 | 210.98 | 0.33 | 0.40 | 399.62 | 170.82 | 0.86 |

**Table S2. Rates of NH4+ oxidation to NO2– + NO3–, NO2– oxidation to NO3–, and NO3– reduction to NO2–at stations PS1. Errors are calculated from the error of the slope of product 15N vs. time.**

| Station | Feature | $NH_4^+$ oxidation (nM/day) | $\sigma$ | product AF slope p-value | $NO_2^-$ oxidation (nM/day) | $\sigma$ | product AF slope p-value | $NO_3^-$ reduction to $NO_2^-$ (nM/day) | $\sigma$ | product AF slope p-value |
|---|---|---|---|---|---|---|---|---|---|---|
| PS1 | Interface | 0.1924 | 0.0004 | 0.00 | 0.00 | 0.00 | 0.65 | 0.000 | 0.000 | 0.51 |
| | Mid-oxycline | 0.52 | 0.0016 | 0.00 | -7.12 | 4.40 | 0.08 | 0.000 | 0.000 | 0.14 |
| | SCM | 0.45 | 0.0020 | 0.00 | 0.00 | 0.00 | 0.68 | 0.000 | 0.000 | 0.91 |
| | Surface | 0.00 | 0.0000 | 0.76 | 0.00 | 0.00 | 0.44 | 0.543 | 0.036 | 0.01 |
| | Top of oxycline | 0.00 | 0.0000 | 0.72 | 0.00 | 0.00 | 0.27 | 0.000 | 0.000 | 0.59 |
| PS2 | Base of ODZ | 0.51 | 0.0872 | 0.05 | 0.00 | 0.00 | 0.16 | 0.000 | 0.000 | 0.69 |
| | Deep ODZ core | 0.00 | 0.0000 | 0.40 | 13.05 | 0.08 | 0.00 | 33.244 | 0.143 | 1.88E-04 |
| | Deep oxycline | 0.27 | 0.0016 | 0.02 | 0.00 | 0.00 | 0.79 | 0.000 | 0.000 | 0.78 |
| | Interface | 2.21 | 0.1675 | 0.00 | 27.01 | 0.49 | 0.01 | 0.000 | 0.000 | 0.60 |
| | PNM | 1.39 | 0.2050 | 0.00 | 0.00 | 0.00 | 0.13 | 0.000 | 0.000 | 0.46 |
| | SCM | 0.00 | 0.0000 | 0.77 | 81.00 | 0.23 | 0.00 | 24.323 | 0.111 | 9.38E-07 |
| | SNM | 0.00 | 0.0000 | 0.95 | 0.00 | 0.00 | 0.30 | 0.000 | 0.000 | 0.20 |
| | Top of oxycline | 0.05 | 0.0013 | 0.04 | 0.00 | 0.00 | 0.17 | 0.000 | 0.000 | 1.00 |
| PS3 | Deep ODZ core | 0.00 | 0.0000 | 0.32 | -271.00 | 15.29 | 0.01 | 10.882 | 0.176 | 0.03 |
| | Deep oxycline | 0.303 | 0.005 | 0.02 | 0.00 | 0.00 | 0.23 | 0.000 | 0.000 | 0.68 |
| | Interface | 0.88 | 0.0645 | 0.00 | 0.00 | 0.00 | 0.60 | 0.000 | 0.000 | 0.16 |
| | Interface2 | 4.68 | 0.07 | 0.00 | 0.00 | 0.00 | 0.29 | 0.000 | 0.000 | 0.44 |
| | Mid-oxycline | 0.00 | 0.0000 | 0.78 | 0.00 | 0.00 | 0.10 | 0.000 | 0.000 | 0.82 |
| | SCM | 0.57 | 0.0706 | 0.02 | 0.00 | 0.00 | 0.12 | 19.201 | 0.133 | 1.30E-07 |
| | SNM | 0.00 | 0.0000 | 1.00 | 465.34 | 86.15 | 0.02 | 0.000 | 0.000 | 0.26 |
| | Top of oxycline | 0.00 | 0.0000 | 0.61 | 0.00 | 0.00 | 0.91 | 0.000 | 0.000 | 0.80 |

**Table S3. Rates of $N_2O$ production from solely $NH_4^+$, $N_2O$ production from $NO_2^-$, $N_2O$ production from $NO_3^-$, and hybrid $N_2O$ production at each experimental depth. production rate error bars are calculated from 100 model optimizations, varying key parameters by up to 25%.**

| Station | Feature | $N_2O$ production from solely $NH_4^+$ (nM/day) | $\sigma$ | $N_2O$ production from $NO_2^-$ (nM/day) | $\sigma$ | $N_2O$ production from $NO_3^-$ (nM/day) | $\sigma$ | Hybrid $N_2O$ production (nM/day) | $\sigma$ | f | $\sigma$ |
|---|---|---|---|---|---|---|---|---|---|---|---|
| PS1 | Interface | 0.00 | 0.00 | 0.0084 | 0.0009 | 1.31 | 0.22 | 0.054 | 0.007 | 0.45 | 0.10 |
| | Mid-oxycline | 0.00 | 0.00 | 0.0015 | 0.0002 | 0.00 | 0.00 | 0.001 | 0.000 | 0.34 | 0.03 |
| | SCM | 1.94E-04 | 1.17E-04 | 0.0013 | 0.0000 | 0.17 | 0.02 | 0.026 | 0.001 | 0.50 | 0.00 |
| | Surface | 0.00 | 0.00 | 0.0000 | 0.0000 | 0.00 | 0.00 | 0.000 | 0.000 | 0.49 | 0.00 |
| | Top of oxycline | 1.18E-05 | 2.46E-06 | 0.0000 | 0.0000 | 0.00 | 0.00 | 0.000 | 0.000 | 0.56 | 0.09 |
| PS2 | Base of ODZ | 0.00 | 0.00 | 0.0125 | 0.0013 | 0.00 | 0.00 | 0.063 | 0.007 | 0.56 | 0.00 |
| | Deep ODZ core | 2.27E-04 | 8.39E-04 | 0.0052 | 0.0003 | 0.21 | 0.04 | 0.006 | 0.007 | 0.23 | 0.24 |
| | Deep oxycline | 0.00 | 0.00 | 0.0000 | 0.0000 | 0.00 | 0.00 | 0.000 | 0.000 | | |
| | Interface | 4.67E-04 | 1.41E-04 | 0.0089 | 0.0003 | 0.07 | 0.01 | 0.039 | 0.008 | 0.19 | 0.14 |
| | PNM | 3.19E-04 | 5.73E-05 | 0.0000 | 0.0000 | 0.01 | 0.00 | 0.001 | 0.000 | 0.52 | 0.06 |
| | SCM | 0.00 | 0.00 | 0.0424 | 0.0011 | 0.72 | 0.12 | 0.053 | 0.013 | 0.38 | 0.13 |
| | SNM | 1.62E-03 | 8.04E-04 | 0.0677 | 0.0087 | 0.32 | 0.05 | 0.006 | 0.002 | 0.44 | 0.09 |
| | Top of oxycline | 9.81E-06 | 4.28E-06 | 0.0000 | 0.0000 | 0.00 | 0.00 | 0.000 | 0.000 | 1.00 | 0.00 |
| PS3 | Deep ODZ core | 1.80E-05 | 3.22E-05 | 0.0134 | 0.0006 | 0.04 | 0.01 | 0.033 | 0.002 | 0.41 | 0.00 |
| | Deep oxycline | 1.39E-04 | 3.54E-05 | 0.0026 | 0.0001 | 0.00 | 0.00 | 0.016 | 0.001 | 0.38 | 0.00 |
| | Interface | 1.56E-05 | 3.73E-05 | 0.0000 | 0.0000 | 0.11 | 0.02 | 0.000 | 0.000 | 0.80 | 0.34 |
| | Interface2 | 1.46E-03 | 8.04E-03 | 0.0088 | 0.0177 | 1.63 | 0.38 | 0.234 | 0.075 | 0.39 | 0.21 |
| | Mid-oxycline | 1.23E-04 | 3.87E-05 | 0.0002 | 0.0000 | 0.00 | 0.00 | 0.000 | 0.000 | 0.00 | 0.01 |
| | SCM | 8.11E-03 | 2.13E-03 | 0.5098 | 0.0346 | 1.63 | 0.26 | 0.152 | 0.020 | 0.33 | 0.15 |
| | SNM | 2.70E-04 | 4.04E-04 | 0.0373 | 0.0061 | 0.68 | 0.10 | 0.050 | 0.039 | 0.94 | 0.15 |
| | Top of oxycline | 2.60E-04 | 5.75E-05 | 0.0001 | 0.0000 | 0.00 | 0.00 | 0.000 | 0.000 | 1.00 | 0.00 |